DEFORMATION OF THE DIASTOLIC LEFT VENTRICLE

I. NONLINEAR ELASTIC EFFECTS

RONALD F. JANZ *and* ARTHUR F. GRIMM

From the Data Processing Subdivision, The Aerospace Corporation, Los Angeles, California 90009, and the Department of Histology, College of Dentistry, and the Department of Physiology, College of Medicine, University of Illinois, Chicago, Illinois 60680

ABSTRACT A linear incremental finite element model is used to analyze the mechanical behavior of the left ventricle. The ventricle is treated as a heterogeneous, nonlinearly elastic, isotropic, thick-walled solid of revolution. A new triaxial constitutive relation for the myocardium is presented which exhibits the observed exponential length-passive tension behavior of left ventricular papillary muscle in the limit of uniaxial tension. This triaxial relation contains three parameters: (*a*) a "small strain" Young's modulus, (*b*) a Poisson's ratio, and (*c*) a parameter which characterizes the nonlinear aspect of the elastic behavior of heart muscle. The inner third and outer two-thirds of the ventricular wall are assumed to have small strain Young's moduli of 30 and 60 g/cm^2, respectively. The Poisson's ratio is assumed to be equal to 0.49 throughout the ventricular wall. In general, the results of this study indicate that while a linearly elastic model for the ventricle may be adequate in terms of predicting pressure-volume relationships, a linear model may have serious limitations with regard to predicting fiber elongation within the ventricular wall. For example, volumes and midwall equatorial circumferential strains predicted by the linear and nonlinear models considered in this study differ by approximately 20 and 90%, respectively, at a transmural pressure of 12 cm H_2O.

INTRODUCTION

In a previous study (Janz and Grimm, 1972), a model for the mechanical behavior of the left ventricle was proposed which included two important characteristics of the ventricle: (*a*) the wall thickness is nonuniform, and (*b*) the composition of the myocardium appears to be heterogeneous. However, the predictions of that model were limited by the assumption that the myocardium is a linearly elastic continuum. In the current study this model is extended to include a nonlinear representation of the elastic behavior of the myocardium. In this representation the effective elastic moduli depend on local deformation. The compliance of the model, therefore, varies significantly with position at elevated transmural pressures. The mathematical formula-

tion of the model is based on the linear incremental finite element method (Mallett and Marcal, 1968).

The geometry of the model considered in this study is identical with the geometry of the model in the previous study. In addition, small deformation elasticity theory is again assumed to be applicable; i.e., strains and rotations are assumed to be small compared with unity and the squares of the rotations are assumed to be negligible compared with the displacement gradients. In the current study, however, the myocardium is assumed to be isotropic throughout the ventricle wall. While these assumptions oversimplify observed anatomical structure and deformation, they do facilitate the computational aspects of the study. A more general model which is not limited by these assumptions is under current development at this laboratory. The predictions of the latter model will be reported at a later date.

Circumferential strain is interpreted as the fractional change in muscle fiber length in the middle layer of the ventricular wall. However, axial strain is interpreted as the fractional change in muscle fiber length in the inner and outer layers of the ventricular wall near the equatorial plane. These interpretations are based on the observations of Streeter et al. with regard to fiber orientation in the canine left ventricle (Streeter et al., 1969).

The predictive capability of the model is illustrated by determining an end diastolic pressure-volume relation for the rat left ventricle as well as the dependence of fiber elongation on transmural pressure at various locations in the ventricular wall. Since the model is a solid of revolution with wall dimensions based on the free wall of the rat left ventricle, predicted fiber elongation should be interpreted as free wall fiber elongation.

METHODS

Experimental Procedures

Serial sections of adult Sprague-Dawley albino male rat hearts are used to determine the free wall geometry of the left ventricle at zero transmural pressure. The rats are anesthesized with sodium pentobarbitol 50 mg/kg of animal weight. The serial sections are obtained from open-chested animals after potassium arrest and formaldehyde solution fixation *in situ*. After formaldehyde solution perfusion the two ventricles are rinsed with distilled water and progressively infiltrated by gelatin solutions of increasing concentration. After 72 h of infiltration in 10% gelatin the gelatin and enclosed heart are refrigerated. After additional formaldahyde solution fixation, frozen serial sections are obtained from the gelatinized heart. The procedure is discussed in more detail by Klein (1970). In general, by eliminating alcohol dehydration, the procedure should more accurately preserve cardiac volumes and shapes before sectioning

The nonlinear elastic behavior of the myocardium is based on the observed length-passive tension behavior of isolated left ventricular papillary muscles of adult Sprague-Dawley albino male rats. The isolated papillary muscle is maintained at 36°C in a bath containing about 300 ml of a bicarbonate-buffered Ringer solution which is oxygenated and stirred by a 99% O_2 – 1% CO_2 gas mixture. Tension levels are measured by means of Grass FT-03 transducer

(Grass Instrument Co., Quincy, Mass.). Muscle lengths are altered by means of a micrometer adjustment. Tension is determined at each length after stress relaxation appears to be complete. (This requires an equilibration of approximately 5 min.)

Triaxial Constitutive Relation

A strain-energy function was constructed in order to characterize mathematically, the nonlinear elastic behavior of the myocardium consistent with the assumption of isotropy. The construction of this function was guided by the following criteria: (*a*) the strain-energy function of an isotropic, elastic material is positive definite, and remains invariant under a permutation in the principal strain components. (*b*) The small strain limiting form of the strain-energy function must correspond to the strain-energy function for an isotropic, linearly elastic material. (*c*) The uniaxial relation between stress and stain implied by the strain-energy function must conform with the observed stress-strain behavior of rat left ventricular papillary muscle under uniaxial tension. It can be demonstrated that the following function satisfies these three criteria:

$$W(\epsilon_1, \epsilon_2, \epsilon_3) = \frac{E}{\beta^2(1+\nu)}\left[\sum_{i=1}^{3} \exp \beta\epsilon_i + \left(\frac{1-2\nu}{\nu}\right) \cdot \exp\left(-\frac{\beta\nu}{1-2\nu}\sum_{i=1}^{3}\epsilon_i\right) - \left(\frac{1+\nu}{\nu}\right)\right], \quad (1)$$

where, E and ν denote the small strain Young's modulus and Poisson's ratio, respectively, and β denotes an additional parameter which is used to characterize the nonlinear elastic behavior of the material. The quantities, ϵ_1, ϵ_2, and ϵ_3 denote the principal components of strain. The expression for strain-energy given by Eq. 1 is cleary invariant under a permutation in the principal components of strain. In addition, this expression defines a positive definite function of strain since it has a global minimum at $\epsilon_1 = \epsilon_2 = \epsilon_3 = 0$.

For relatively small values of strain (or β) Eq. 1 reduces to the form:

$$W(\epsilon_1, \epsilon_2, \epsilon_3) \simeq \frac{E}{2(1+\nu)}\left[\sum_{i=1}^{3}\epsilon_i^2 + \frac{\nu}{1-2\nu}\left(\sum_{i=1}^{3}\epsilon_i\right)^2\right], \quad (2)$$

which is the familiar strain-energy function for an isotropic, linearly elastic material

According to the principle of virtual work, the principal stress field may be determined from the strain-energy function W as follows:

$$\sigma_i = \partial W/\partial\epsilon_i, \qquad i = 1, 2, 3, \quad (3)$$

were σ_i denotes the ith principal component of stress. The stress field corresponding to the strain-energy function defined in Eq. 1 is then given by:

$$\sigma_i = \frac{E}{\beta(1+\nu)}\left[\exp \beta\epsilon_i - \exp\left(-\frac{\beta\nu}{1-2\nu}\sum_{j=1}^{3}\epsilon_j\right)\right], \qquad i = 1, 2, 3. \quad (4)$$

Under uniaxial load, defined by the conditions:

$$\epsilon_1 = \epsilon$$

$$\epsilon_2 = \epsilon_3 = -\nu\epsilon, \tag{5}$$

where ϵ denotes strain in a direction coincident with the load direction, σ_1 becomes:

$$\sigma = [E/\beta(1 + \nu)](e^{\beta\epsilon} - e^{-\beta\nu\epsilon}), \tag{6}$$

and σ_2 and σ_3 are both equal to zero. It will be shown later that an expression of the form given by Eq. 6 is representative of the observed uniaxial stress-strain behavior of passive rat left ventricular papillary muscle.

The relations between stress and strain defined by Eq. 4 are used to characterize the elastic behavior of the rat myocardium in this study. However, in order to determine stress and strain in the ventricular wall (assumed to deform axisymmetrically) it is desirable to relate the components of stress and strain in the datum (cylindrical) coordinate system of the left ventricle rather than the principal coordinate system which depends on position. This can be accomplished by using the law of transformation for the stress tensor which may be stated in the following way:

$$\{\sigma\}_{rz\theta} = [L]^T\{\sigma\}_{123}, \tag{7}$$

where,

$$\{\sigma\}_{rz\theta} = \begin{bmatrix} \sigma_{rr} \\ \sigma_{zz} \\ \sigma_{\theta\theta} \\ \tau_{rz} \end{bmatrix}, \qquad \{\sigma\}_{123} = \begin{bmatrix} \sigma_1 \\ \sigma_2 \\ \sigma_3 \end{bmatrix},$$

and

$$[L]^T = \begin{bmatrix} \cos^2\phi & \sin^2\phi & 0 \\ \sin^2\phi & \cos^2\phi & 0 \\ 0 & 0 & 1 \\ \cos\phi\sin\phi & -\cos\phi\sin\phi & 0 \end{bmatrix}.$$

The quantities σ_{rr}, σ_{zz}, $\sigma_{\theta\theta}$, τ_{rz} denote the four nonzero coponents of stress in axisymmetric deformation. The quantities σ_1, σ_2, σ_3 denote the principal components of stress and ϕ denotes the angle through which the principal coordinate system would have to be rotated in order to coincide with the datum coordinate system. The relations defined by Eq. 7 are of the desired form, namely,

$$\sigma_{rr} = \sigma_{rr}(\epsilon_{rr}, \epsilon_{zz}, \epsilon_{\theta\theta}, \gamma_{rz}),$$

$$\sigma_{zz} = \sigma_{zz}(\epsilon_{rr}, \epsilon_{zz}, \epsilon_{\theta\theta}, \gamma_{rz}),$$

$$\sigma_{\theta\theta} = \sigma_{\theta\theta}(\epsilon_{rr}, \epsilon_{zz}, \epsilon_{\theta\theta}),$$

$$\tau_{rz} = \tau_{rz}(\epsilon_{rr}, \epsilon_{zz}, \epsilon_{\theta\theta}), \tag{8}$$

where ϵ_{rr}, ϵ_{zz}, $\epsilon_{\theta\theta}$, γ_{rz} denote the four nonzero components of strain in axisymmetric deformation. The explicit dependence of stress on the strain components indicated by Eqs. 8 follows from the fact that σ_i, $i = 1, 2, 3$ are related to ϵ_i, $i = 1, 2, 3$ by Eq. 4 and,

$$\epsilon_1 = \tfrac{1}{2}\{\epsilon_{rr} + \epsilon_{zz} + [(\epsilon_{rr} - \epsilon_{zz})^2 + \gamma_{rz}^2]^{1/2}\},$$

$$\epsilon_2 = \tfrac{1}{2}\{\epsilon_{rr} + \epsilon_{zz} - [(\epsilon_{rr} - \epsilon_{zz})^2 + \gamma_{rz}^2]^{1/2}\},$$

$$\epsilon_3 = \epsilon_{\theta\theta},$$

$$\phi = \tfrac{1}{2}\tan^{-1}\frac{\gamma_{rz}}{\epsilon_{rr} - \epsilon_{zz}}.$$

The jacobian matrix, $[J]$, associated with Eqs. 8 is defined by:

$$[J] = \begin{bmatrix} \dfrac{\partial\sigma_{rr}}{\partial\epsilon_{rr}} & \dfrac{\partial\sigma_{rr}}{\partial\epsilon_{zz}} & \dfrac{\partial\sigma_{rr}}{\partial\epsilon_{\theta\theta}} & \dfrac{\partial\sigma_{rr}}{\partial\gamma_{rz}} \\ & \dfrac{\partial\sigma_{zz}}{\partial\epsilon_{zz}} & \dfrac{\partial\sigma_{zz}}{\partial\epsilon_{\theta\theta}} & \dfrac{\partial\sigma_{zz}}{\partial\gamma_{rz}} \\ \text{SYMMETRIC} & & \dfrac{\partial\sigma_{\theta\theta}}{\partial\epsilon_{\theta\theta}} & \dfrac{\partial\sigma_{\theta\theta}}{\partial\gamma_{rz}} \\ & & & \dfrac{\partial\tau_{rz}}{\partial\gamma_{rz}} \end{bmatrix}. \tag{9}$$

The relevance of the jacobian matrix can be made more apparent by expanding Eqs. 8 in a four-dimensional Taylor series about some specified value of the strain vector, ${}_{n-1}\{\epsilon\}_{rz\theta}$. It can be shown that:

$${}_n\{\sigma\}_{rz\theta} = {}_{n-1}\{\sigma\}_{rz\theta} + {}_{n-1}[J]_n\{\delta\epsilon\}_{rz\theta} + \ldots, \tag{10}$$

where, ${}_{n-1}\{\sigma\}_{rz\theta}$ and ${}_{n-1}[J]$ denote the stress vector and jacobian matrix, respectively, evaluated at ${}_{n-1}\{\epsilon\}_{rz\theta}$. ${}_n\{\sigma\}_{rz\theta}$ denotes the stress vector evaluated at some other value of the strain vector denoted by ${}_n\{\epsilon\}_{rz\theta}$ and ${}_n\{\delta\epsilon\}_{rz\theta} = {}_n\{\epsilon\}_{rz\theta} - {}_{n-1}\{\epsilon\}_{rz\theta}$. It is clear from Eq. 10 that the jacobian matrix characterizes the compliance of the material under investigation for small perturbations in strain about a predetermined value.

Specification of the Elastic Constants E, ν, and β

For small values of uniaxial strain ($\epsilon \ll 1$) Eq. 6 simplifies to the following form:

$$\sigma \simeq E\epsilon + O(\epsilon^2). \tag{11}$$

E is therefore referred to as the small strain modulus. For rat left ventricular papillary muscle this modulus is approximatly equal to 60 g/cm^2. The small strain modulus in the outer two-thirds of the left ventricular wall is assumed to be equal to this value. This assumption is based on the observation that muscle fibers in this region appear to be densely packed. The small strain Young's modulus in the inner third of the ventricular wall is assumed to be equal to 30 g/cm^2. The latter somewhat arbitrary choice of modulus is based on the observation that sinusoidal-like spaces containing blood compose approximately 30–50 % of the wall volume in the vicinity of the endocardium. Assuming this combination of muscle and blood behaves mechanically like a porous composite, the effective Young's modulus of the ventricular wall near the endocardium is probably equal to approximately one-half that of the muscle matrix (Ishai and Cohen, 1967).

The myocardium is assumed to be essentially incompressible with a Poisson's ratio (ν) equal to 0.49. The nonlinear behavior of the myocardium is characterized by the parameter β. This parameter is obtained by fitting Eq. 6 to uniaxial length-tension data for rat left ventricular papillary muscle. In order to do this the undeformed cross-sectional area A_0, optimum force F_{opt}, and unloaded length l_0 of the papillary muscle are required. Typically, $A_0 \simeq 1$ mm^2, $F_{opt} \simeq 2.5$ g, and $l_0 \simeq 0.8\ l_{opt}$, where l_{opt} denotes fiber length when developed force is optimal (Grimm et al. 1970). Eq. 6 may be transformed into a relationship between force and length as follows:

$$\frac{F}{F_{opt}} = \frac{EA_0}{F_{opt}\beta(1+\nu)}\,(e^{\beta\epsilon} - e^{-\beta\nu\epsilon}), \tag{12}$$

where, ϵ is defined by:

$$\epsilon = \frac{(l/l_{opt}) - (l_0/l_{opt})}{l_0/l_{opt}}, \tag{13}$$

and, l denotes muscle length when passive muscle tension is equal to F.

Substituting the numerical values given above for A_0, l_0 and F_{opt} into Eqs. 12 and 13, it follows that Eq. 6 is equivalent to the following length-passive tension relation:

$$\frac{F}{F_{opt}} = \frac{0.004E}{\beta(1+\nu)}\{\exp(\beta[1.25(l/l_{opt}) - 1]) - \exp(-\nu\beta[1.25(l/l_{opt}) - 1])\}. \tag{14}$$

The only undetermined parameter in Eq. 14 is β since E and ν are equal to 60 g/cm^2 and 0.49, respectively. As indicated in Fig. 1, Eq. 14 provides an excellent fit to observed data (at least for values of l/l_{opt} between 0.8 and 1.0) with β equal to 15.

A summary of the numerical values chosen for the elastic constants in this study is given in Table I. As indicated in the table, ν and β were assumed to be independent of position.

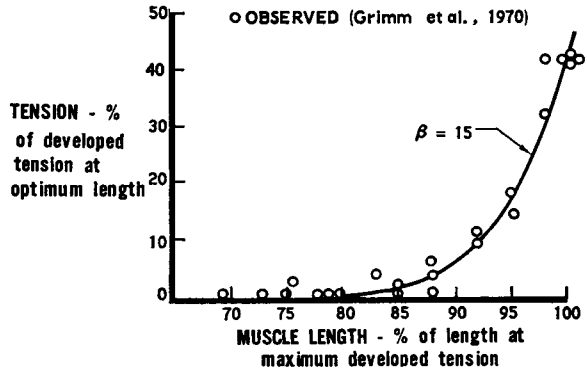

FIGURE 1 Passive tension-length relation for rat papillary muscle. The parameter β was determined by fitting Eq. 14 to the observed data in this figure. The solid curve represents a graph of Eq. 14 with $\beta = 15$. The parameter β characterizes the nonlinear aspect of the elastic behavior of the papillary muscle.

TABLE I

ASSUMED MYOCARDIAL ELASTIC CONSTANTS

	Left Ventricular Wall	
	Inner third	Outer two-thirds
E (g/cm^2)	30	60
ν	0.49	0.49
β	15	15

Incremental Procedure

The incremental procedure used in this study is one of several possible procedures reviewed by Mallett and Marcal (1968) for treating nonlinear structures. These authors considered the case of nonlinear (geometric) deformation of a linearly elastic material. The procedure is equally valid for the case treated here, namely, nonlinear (material) deformation of an elastic solid which is geometrically linear (small strains and displacements).

In this procedure the load on the structure is applied in incremental steps. Deformation is assumed to be linearly elastic during each step. The strain-dependent elastic moduli for the current step are based on values of accumulated strain determined from previous steps.

The resulting equations of equilibrium for the finite element idealization of the left ventricle are linear and of the form:

$$ {}_{n-1}[K]_n\{\delta u\} = {}_n\{\delta Q\}, \qquad n = 1, 2, \ldots, N \tag{15} $$

where, ${}_{n-1}[K]$ is the stiffness matrix for the finite element model defined in terms of the jacobian matrix (Eq. 9) evaluated at the $(n-1)$th loading step. ${}_n\{\delta u\}$ denotes the change in the nodal displacement vector for the model at the nth loading step.

${}_n\{\delta Q\}$ denotes the load vector defined in terms of the nth increment in load applied to the model and N denotes the total number of loading steps.

The magnitude of the numerical error introduced by representing the exact nonlinear equilibrium equations by the sequence of linear equations defined in Eq. 15 can be controlled by appropriate adjustment of the load increments. As pointed out by Mallett and Marcal (1968) some numerical experimentation is required in order to determine a loading step size which is adequate for a given problem. Several test cases were examined in order to evaluate the procedure. These cases consisted of thick-walled hollow spheres loaded internally with various hydrostatic pressures. The nonlinear constitutive relationship discussed earlier was used to represent the elastic behavior of the sphere. It does not appear that the deformation of this nonlinear sphere can be determined analytically. However, the equilibrium equations can be formulated in terms of two first-order nonlinear differential equations in the radial and circumferential components of strain (Appendix 1). These equations together with two nonlinear boundary conditions in the strain components at the interior and exterior surfaces of the sphere can be solved numerically using a modified Runge-Kutta procedure. The same cases were treated using the incremental finite element procedure with constant load increments of 1 cm H_2O.

As indicated in Fig. 2, at an internal pressure of 15 cm H_2O it was found that the two procedures yielded radial and circumferential strain distributions through the wall of the sphere which agreed to within 2% independent of position. It was therefore concluded that a loading step size of 1 cm H_2O was sufficiently small for the purpose of this study and all results presented correspond to this value.

Stress and strain for each finite element are accumulated in the following manner:

$$
\begin{aligned}
{}_n\{\sigma\}^m_{rz\theta} &= {}_{n-1}\{\sigma\}^m_{rz\theta} + {}_{n-1}[J]^m\,{}_n\{\delta\epsilon\}^m_{rz\theta}\,,\\
{}_n\{\epsilon\}^m_{rz\theta} &= {}_{n-1}\{\epsilon\}^m_{rz\theta} + {}_n\{\delta\epsilon\}^m_{rz\theta}\,,\\
n &= 1, 2, \ldots N,
\end{aligned}
$$

where, the superscript m denotes the mth finite element in the model. ${}_0\{\sigma\}_{rz\theta} = {}_0\{\epsilon\}_{rz\theta} = 0$ and ${}_0[J]^m$ denotes the small-strain limiting form of the jacobian matrix which can easily be shown to be of the form:

$$
{}_0[J]^m = \frac{E}{(1+\nu)(1-2\nu)}
\begin{bmatrix}
1-\nu & \nu & \nu & 0 \\
 & 1-\nu & \nu & 0 \\
 & & 1-\nu & 0 \\
\text{SYMMETRIC} & & & \dfrac{1-2\nu}{2}
\end{bmatrix},
$$

where, E denotes the small strain Young's modulus and ν denotes Poisson's ratio.

A planar view of the finite element model for the left ventricle is shown in Fig. 3.

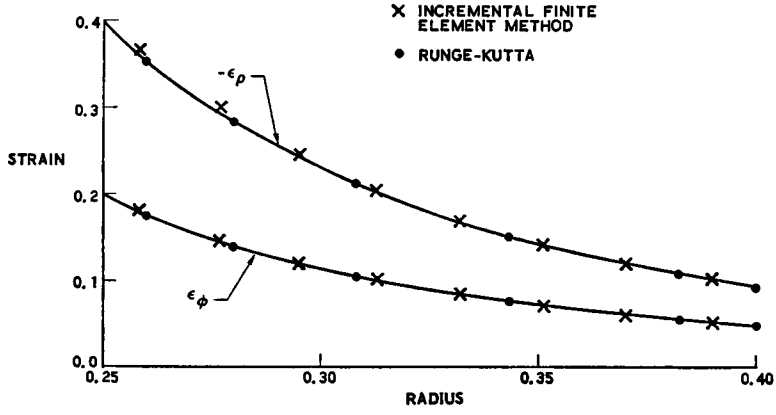

FIGURE 2 Comparison of an incremental finite element solution with a Runge-Kutta solution for a hollow homogeneous sphere. The undeformed inner radius is equal to 0.25, the undeformed outer radius is equal to 0.40 and the interior pressure is equal to 15 g/cm². In addition, $E = 60$ g/cm², $\nu = 0.49$, and $\beta = 15$.

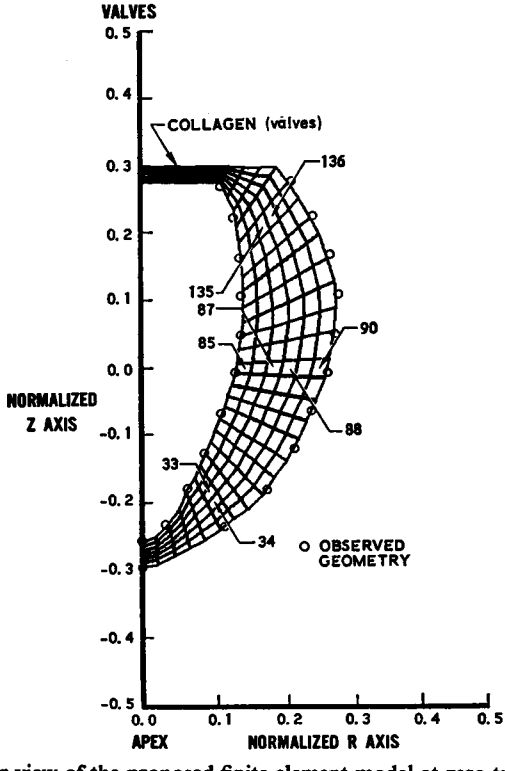

FIGURE 3 A planar view of the proposed finite element model at zero transmural pressure. In axisymmetric deformation the equations of equilibrium involve only axial (z) and radial (r) components of displacement. All stresses and strains are determined from deformation in the r-z plane. The numbered elements indicate specific locations referred to in Figs. 7 and 8.

As indicated in this figure, the free wall geometry of the potassium arrested rat left ventricle at a transmural pressure equal to 0 cm H_2O defines the geometry of the model. There are 198 finite elements in the model, each of which has a quadrilateral cross section. This subdivision was maintained under all loading conditions discussed. (Elements 85, 87, 88, and 90 in the equatorial plane, as well as elements 33, 34, 87, 88, 135, 136 which are adjacent to the midwall meridian are examined in more detail later in the discussion.) The computer program which is used to compute stress and strain in each element of this model is based on a program which was developed at this laboratory (Jones and Crose, 1968). Numerical results obtained with this program are presented in the next section.

RESULTS AND DISCUSSION

The rat left ventricular end diastolic pressure-volume relation predicted by the nonlinear model developed in this study is illustrated in Fig. 4. (The procedure for determining volumes is summarized in Appendix II.) Below a pressure of 4 cm H_2O the curve is concave downward. However, there is a point of inflection in the neighborhood of 4 cm H_2O. Above this pressure, the pressure-volume relationship reflects the pronounced decrease in material compliance which is apparent in the

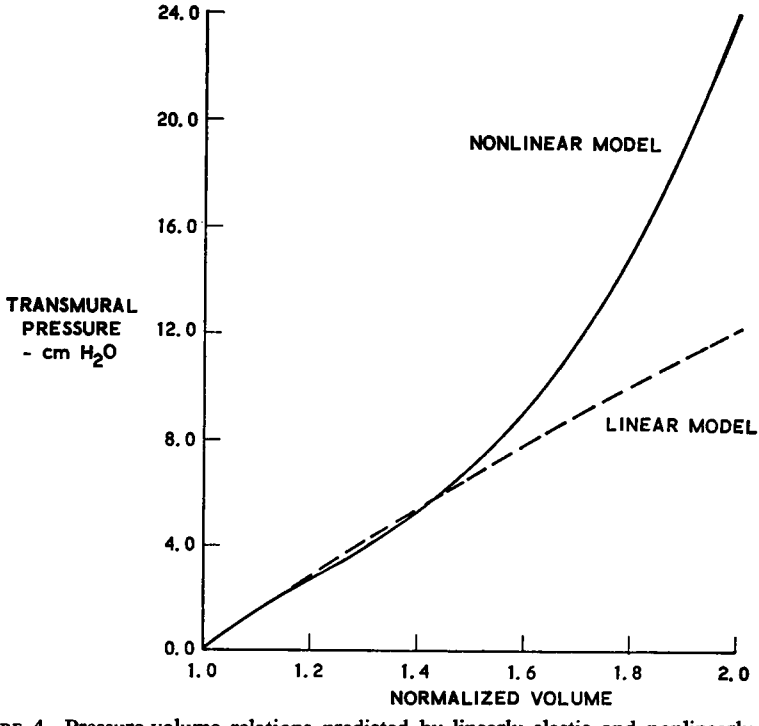

FIGURE 4 Pressure-volume relations predicted by linearly elastic and nonlinearly elastic models for the rat left ventricle. Nonlinear elastic effects become increasingly important with increasing transmural pressure above 6 cm H_2O.

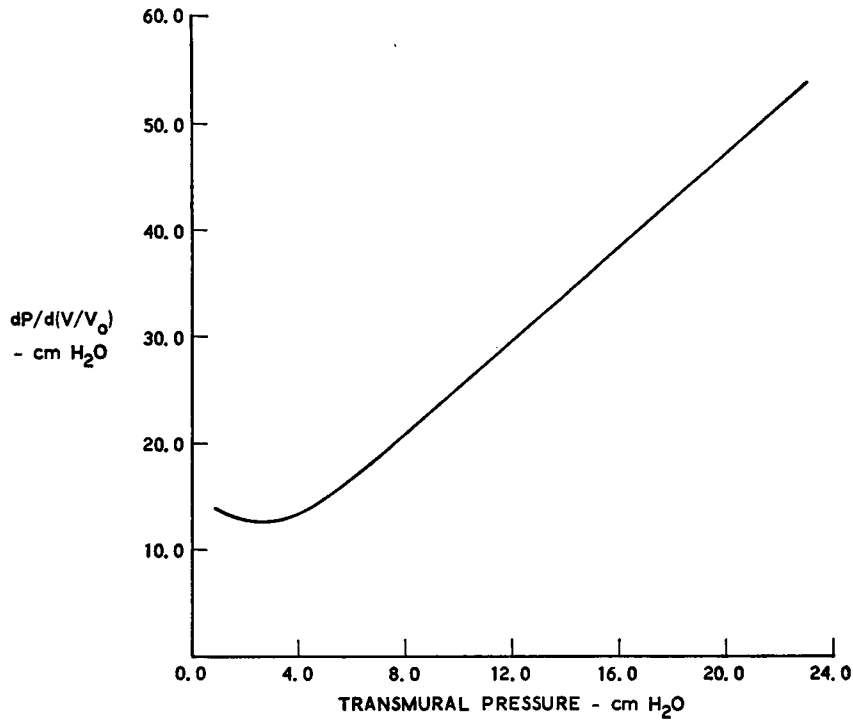

FIGURE 5 The slope (stiffness) of the nonlinear pressure-volume relation given in Fig. 4 plotted as a function of transmural pressure. Below a pressure of 6 cm H_2O the relation is nonlinear. Above this pressure the relation appears to be linear.

passive papillary muscle length-tension relationship. This result is consistent with the observed variation in passive compliance of the canine left ventricle (Spotnitz et al., 1966; Diamond et al., 1971).

The pressure-volume relation predicted by a model which is based on a linearly elastic representation of the rat myocardium is also illustrated in Fig. 4. The "linear" model consists of a finite element representation of the rat left ventricle in which the elastic behavior of the myocardium is represented by the small strain limiting form of the nonlinear constitutive relation discussed earlier; i.e., in the linear model the myocardium is assumed to be isotropic with a Young's modulus in the inner third of the ventricular wall equal to 30 g/cm², a Young's modulus in the outer two-thirds of the ventricular wall equal to 60 g/cm², and a Poisson's ratio equal to 0.49 throughout the ventricular wall. As indicated in Fig. 4 the pressure-volume relations predicted by the two models agree very well up to a transmural pressure of 6 cm H_2O. However, with increasing transmural pressure above this value, the nonlinear model predicts a significant reduction in ventricular compliance.

The normalized slope of the presure-volume curve predicted by the nonlinear model is plotted as a function of transmural pressure in Fig. 5. Above a pressure of 6 cm H_2O the predicted stiffness appears to be a linear function of transmural pressure.

This implies that there is an exponential relationship between pressure and volume for pressures above this value. Relatively large increments in pressure above the normal range in end diastolic pressure for the rat therefore appear to be required in order to alter ventricular geometry and therefore end diastolic fiber length. The slope of the linear portion of this curve is approximately 18% greater than the slope of comparable data repoted by Diamond et al. (1971) for the canine left ventricle.

Fig. 6 illustrates midwall circumferential strain in the equatorial plane predicted by the linear and nonlinear models discussed above. As indicated in this figure, with increasing transmural pressure above 2 cm H_2O the nonlinear model predicts significantly less strain than the linear model. Comparing Figs. 4 and 6, it is clear that while the volumes predicted by the linear and nonlinear models agree to within 20% at a transmural pressure of 12 cm H_2O (well within the "normal" range in end diastolic pressures for the rat) the midwall, equatorial circumferential strains predicted by the two models differ by over 90% at this pressure.

Fig. 7 illustrates the predicted dependence of axial strain in elements 85 and 90 and average circumferential strain in elements 87 and 88 on transmural pressure. (Fig. 3 illustrates the positions of these finite elements. Since all muscle fibers are assumed to be axially oriented in the inner and outer layers at the equatorial plane, axial strain is used as a measure of fiber elongation at these locations. At the midwall meridian, all muscle fibers are assumed to be circumferentially oriented and circumferential strain is used as a measure of fiber elongation.) At transmural pressures

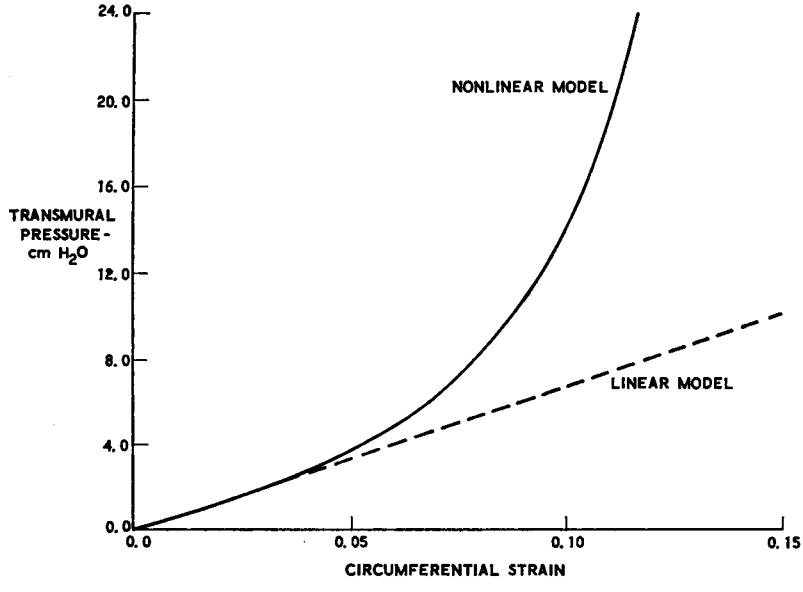

FIGURE 6 Average circumferential strain in elements 87 and 88 predicted by linearly elastic and nonlinearly elastic models for the rat left ventricle. Nonlinear elastic effects become increasingly important with increasing transmural pressure above 2 cm H_2O.

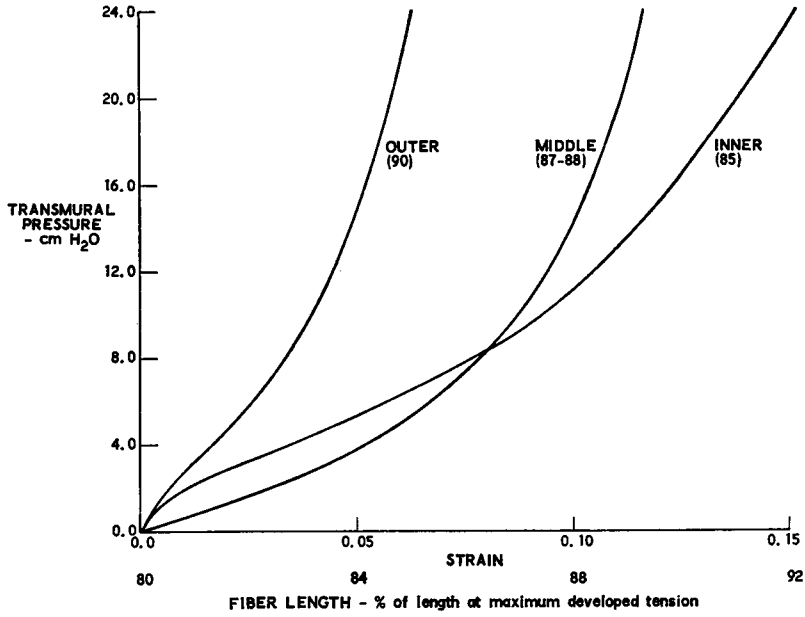

FIGURE 7 Predicted fiber deformation near the equatorial plane at the numbered positions given in Fig. 3. Transmural pressure is plotted as a function of axial strain in elements 85 and 90 and the average value of circumferential strain in elements 87 and 88.

greater than 9 cm H_2O the model predicts a monotonic increase in muscle fiber elongation from the epicardium to the endocardium of the ventricular wall consistent with sarcomere length data obtained by Spotnitz et al. (1966) for the canine left ventricle. For example, at a transmural pressure of 24 cm H_2O, predicted fiber lengths in the outer, middle, and inner layers of the ventricular wall are equal to 85, 89, and 92%, respectively, of the optimum length for the development of maximum isometric tension. (This result is based on the assumption that muscle fiber length at zero transmural pressure is equal to 80% of the optimum length independent of position in the ventricular wall, see Fig. 1.) However, at transmural pressures less than 8 cm H_2O, the model predicts greater elongation of the circumferentially oriented muscle fibers in the middle layer of the ventricular wall than axially oriented muscle fibers in the inner layer.

Fig. 8 illustrates the predicted dependence of the average circumferential strain in elements 33 and 34, 87 and 88, and 135 and 136 on transmural pressure. (Fig. 3 illustrates the positions of these finite elements. Since all muscle fibers are assumed to be circumferentially oriented at the middle surface, circumferential strain is used as a measure of fiber elongation at all three positions indicated in Fig. 8.) According to the model the greatest amount of fiber elongation will occur near the apex of the ventricle and the least amount of fiber elongation will occur between the base and equator. At a transmural pressure of 24 cm H_2O, predicted fiber lengths at the mid-

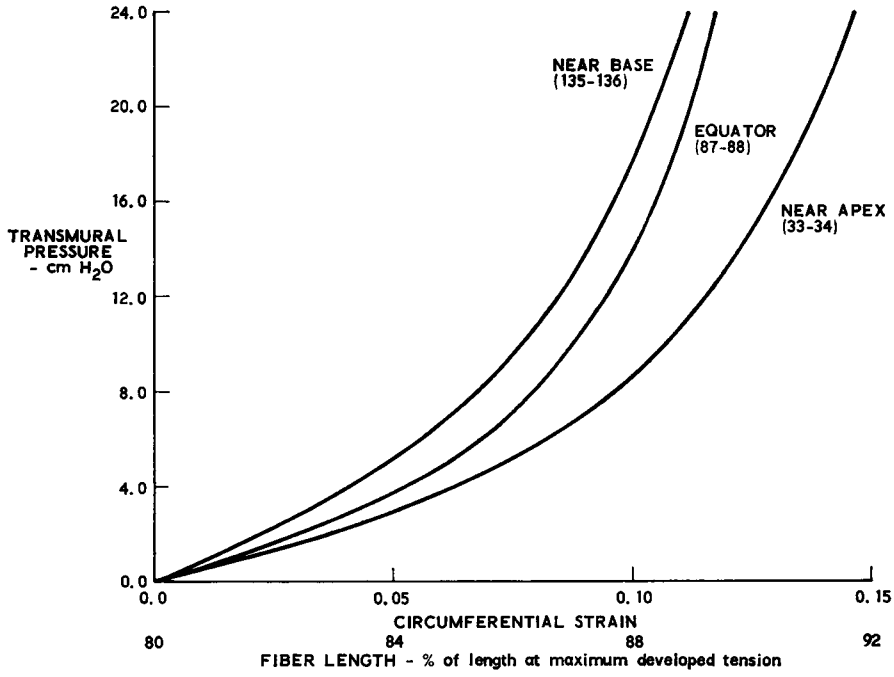

FIGURE 8 Predicted fiber deformation near the middle surface at the numbered positions given in Fig. 3. Transmural pressure is plotted as a function of average circumferential strain in each of the two adjacent elements indicated in this figure.

dle surface near the apex and base are equal to 92 and 89%, respectively, of the optimum length for the development of maximum isometric tension. Fig. 8 also illustrates two further implications of the model. First, since the normal range of end diastolic transmural pressures in the rat left ventricle varies between approximately 7 and 14 cm H_2O, end diastolic fiber length in the middle layer of the ventricular wall may normally be less than 90% of the optimum length for the development of peak systolic tension. Second, even though an increase in transmural pressure above 14 cm H_2O results in a more favorable length for the development of active tension, the resulting changes in length are small. For example, an increase in transmural pressure of more than 70% is required to increase the length of a midwall muscle fiber in the equatorial plane by 1.5%. This corresponds to an increase in the potential isometric tension developed by this fiber of approximately 13%.

All of the results discussed in this section indicate the importance of the nonlinear elastic behavior of the myocardium as a determinant of the state of deformation in the end diastolic left ventricle. The primary assumptions in the model are that muscle fibers in the ventricular wall have the same elastic properties as isolated left ventricular papillary muscle and that at zero transmural pressure the ventricle is in an unstressed, unstrained state. Additional assumptions of isotropy and axisymmetric deformation are made to simplify the analysis.

APPENDIX I

Thick-Walled Hollow Sphere Test Case

The equation of equilibrium for spherically symmetric deformation is given by:

$$(d\sigma_\rho/d\rho) + 2(\sigma_\rho - \sigma_\phi)/\rho = 0, \tag{A1}$$

where, σ_ρ equals the radial stress, and σ_ϕ equals the circumferential stress. The boundary conditions of interest are as follows:

$$\begin{aligned} \sigma_\rho(a) &= -P, \\ \sigma_\rho(b) &= 0, \end{aligned} \tag{A2}$$

where, a equals the interior radius of sphere, b equals the exterior radius of sphere, and P equals the interior hydrostatic pressure.

Two first-order differential equations in radial strain (ϵ_ρ) and circumferential strain (ϵ_ϕ) may be obtained by introducing the kinematic relations and the stress-strain relations:

$$\epsilon_\rho = du/d\rho, \tag{A3}$$

$$\epsilon_\phi = u/\rho, \tag{A4}$$

where, u equals the radial displacement

$$\sigma_\rho = \frac{E}{\beta(1+\nu)}\left\{\exp \beta\epsilon_\rho - \exp\left[\frac{-\beta\nu}{1-2\nu}(\epsilon_\rho + 2\epsilon_\phi)\right]\right\}, \tag{A5}$$

$$\sigma_\phi = \frac{E}{\beta(1+\nu)}\left\{\exp \beta\epsilon_\phi - \exp\left[\frac{-\beta\nu}{1-2\nu}(\epsilon_\rho + 2\epsilon_\phi)\right]\right\}. \tag{A6}$$

Eqs. A 3 and A 4 imply,

$$d\epsilon_\phi/d\rho = (\epsilon_\rho - \epsilon_\phi)/\rho. \tag{A7}$$

Substituting Eqs. A 5 and A 6 into Eq. A 1 rearranging,

$$\frac{d\epsilon_\rho}{d\rho} = \frac{-2\left\{\frac{1}{\beta\rho}(\exp \beta\epsilon_\rho - \exp \beta\epsilon_\phi) + \frac{\nu}{1-2\nu}\exp\left[\frac{-\beta\nu}{1-2\nu}(\epsilon_\rho + 2\epsilon_\phi)\right]\frac{d\epsilon_\phi}{d\rho}\right\}}{\exp \beta\epsilon_\rho + \frac{\nu}{1-2\nu}\exp\left[\frac{-\beta\nu}{1-2\nu}(\epsilon_\rho + 2\epsilon_\phi)\right]}. \tag{A8}$$

Eqs. A 7, A 8, and A 2 were solved using a modified Runge-Kutta procedure. A typical solution is compared with an incremental finite element solution in Fig. 2.

APPENDIX II

Determination of the Interior Volume of the Model

The deformed coordinates (r_i, z_i) of the ith nodal ring on the inner surface of the model are determined from the undeformed coordinates $(\tilde{r}_i, \tilde{z}_i)$ in the following way:

$$r_i = \tilde{r}_i + \sum_{j=1}^{n} {}_j\delta u_{ri}, \tag{A9}$$

$$z_i = \tilde{z}_i + \sum_{j=1}^{n} {}_j\delta u_{zi}, \qquad (A\ 10)$$

where, ${}_j\delta u_{ri}$ and ${}_j\delta u_{zi}$ refer to the radial and axial increments in displacement determined from Eq. 15 for the ith nodal ring at the jth loading step.

As indicated in Fig. 3, the lumen cross-sectional area is represented by a polygon with vertices determined by these nodal rings. The lumen volume is obtained by revolving this area about the apex-valve axis. It can easily be shown that the r coordinate of the centroid ($\bar{r}$) of this area is given by:

$$\begin{aligned} \bar{r} &= \frac{1}{6A}\left|\sum_{i=1}^{n}(z_{i+1} - z_i)(r_{i+1}^2 + r_i r_{i+1} + r_i^2)\right|, \\ &= \frac{1}{6A}\left|\sum_{i=1}^{n}(r_i z_{i+1} - r_{i+1} z_i)(r_i + r_{i+1})\right|, \end{aligned} \qquad (A\ 11)$$

where r_{n+1} and z_{n+1} are defined to be equal to r_1 and z_1, respectively. The quantity A denotes the cross-sectional area of the lumen. The lumen volume (V) is then determined from the expression:

$$V = 2\pi\bar{r}A. \qquad (A\ 12)$$

This investigation was supported by the U. S. Public Health Service research grant no. HL-14651 from the National Heart and Lung Institute and U. S. Public Health Service research grant no. DE-02417 from the National Institute of Dental Research.

Received for publication 8 December 1972.

REFERENCES

DIAMOND, G., J. S. FORRESTER, J. HARGIS, W. W. PARMLEY, R. DANZIG, and H. J. C. SWAN. 1971. *Circ. Res.* **29**:267.

GRIMM, A. F., K. V. KATELE, R. KUBOTA, and W. V. WHITEHORN. 1970. *Am. J. Physiol.* **218**:1412.

ISHAI, O., and L. J. COHEN. 1967. *Int. J. Mech. Sci.* **9**:539.

JANZ, R. F., and A. F. GRIMM. 1972. *Circ. Res.* **30**:244.

JONES, R. M., and J. G. CROSE. 1968. SAAS-II Finite Element Stress Analysis of Axisymmetric Solids with Orthotropic, Temperature-Dependent Material Properties. The Aerospace Corporation, Los Angeles. TR-0200(S4980)-1.

KLEIN, S. A. 1970. Morphologic Patterns in the Growing Rat Heart. M.S. Thesis. University of Illinois, Chicago.

MALLETT, R. H., and P. V. MARCAL. 1968. *J. Struc. Div. ASCE* 94 ST 9:2081.

SPOTNITZ, H. M., E. H. SONNENBLICK, and D. SPIRO. 1966. *Circ. Res.* **18**:49.

STREETER, D. D., JR., H. M. SPOTNITZ, D. P. PATEL, J. ROSS, JR., and E. H. SONNENBLICK. 1969. *Circ. Res.* **24**:339.